Suppression of metal-to-insulator transition and appearance of superconductivity in $Cu_{1-x}Zn_xIr_2S_4$

Guanghan Cao,* Takao Furubayashi, Hiroyuki Suzuki, Hideaki Kitazawa,† and Takehiko Matsumoto
National Institute for Materials Science, Sengen 1-2-1, Tsukuba, Ibaraki 305-0047, Japan

Yoshiya Uwatoko
The Institute for Solid State Physics, University of Tokyo, Kashiwa, Chiba 277-8581, Japan
(Received 7 August 2000; published 13 November 2001)

The thiospinel system $Cu_{1-x}Zn_xIr_2S_4$ ($0 \leqslant x \leqslant 0.9$) has been studied by x-ray diffraction, electrical resistivity, and magnetic susceptibility measurements. The parent compound $CuIr_2S_4$, being metallic at room temperature, undergoes a structural phase transition towards lower symmetry around 230 K and becomes an insulator at the low temperature. The Zn substitution for Cu was found to drastically suppress the metal-to-insulator (MI) transition, resulting in the appearance of superconductivity. The MI transition temperature T_{MI} and the extent of the structural distortion both decrease with increasing x until the phase transition is completely suppressed at $x \sim 0.4$. In the region of $x \leqslant 0.4$, the cubic spinel phase coexists with the low-symmetry phase below T_{MI}. For the metallic phase, the change of the Pauli paramagnetic susceptibility indicates the hole-filling mechanism due to an excess electron from the Zn substitution for Cu. The insulating state of the low-symmetry phase is tentatively explained in terms of charge ordering combined with the Ir^{4+} dimerization. Bulk type-II superconductivity below 3.4 K is observed for $0.25 \leqslant x \leqslant 0.8$ samples. The superconducting transition temperature decreases with increasing the Zn content. The abnormal behavior of the normal-state resistivity below 200 K for $0.3 \leqslant x \leqslant 0.5$ samples suggests modification of the electronic states, which might be related to the occurrence of superconductivity.

DOI: 10.1103/PhysRevB.64.214514 PACS number(s): 71.30.+h, 74.70.Dd, 72.80.Ga, 75.20.Ck

I. INTRODUCTION

Spinel chalcogenides AB_2X_4 have been extensively studied for their various physical properties in the past few decades.[1] Recently, $CuIr_2S_4$ was discovered to exhibit an interesting metal-to-insulator (MI) transition at $T_{MI} \sim 230$ K, accompanied by a structural phase transition towards lower symmetry.[2–4] This finding has stimulated some renewed interest in the area.[5–13]

The high-temperature metallic (HTM) $CuIr_2S_4$ phase crystallizes in a normal cubic spinel structure with Cu and Ir occupying the A and B sites, respectively. The low-temperature insulating (LTI) phase was proposed to be a deformed spinel with the tetragonal symmetry by stretching along [001] direction and correspondingly compressing the other two dimensions.[3] Compared with the cubic phase, it has a volume contraction of 0.7%. The axial ratio $c_t/\sqrt{2}a_t$, where c_t and a_t are the tetragonal lattice constants, was determined as 1.033 at 10 K. In addition, unidentified superstructure was suggested from a few extra reflections in the low-temperature x-ray diffraction (XRD) pattern. Very recently, it was suggested that the low-symmetry phase was triclinic by a synchrotron radiation XRD measurement.[5] However, the details of the crystal structure is still in progress. As an approximation, the tetragonal structure model will still be employed in this paper.

At the MI transition, a sudden increase in the electrical resistivity occurs with decreasing temperature. Meanwhile, the magnetic susceptibility shows a sharp drop from paramagnetism in the metallic state to diamagnetism for the insulating phase. No intrinsic magnetic moment has been observed in the LTI phase. A photoemission spectrum study[6] and optical conductivity spectrum measurement[7] revealed a small band-gap opening at the Fermi level (E_F) for the MI transition. Band-structure calculations[8] succeeded in elucidating the metallic state with hole conduction for the cubic phase. However, it does not give an insulating electronic state for the tetragonal structure. Most interestingly, it was found that the external pressure stabilized the insulating phase rather than the metallic one.[3,9] This is in contradiction with the general idea that the applied pressure should lead to a metallization by enhancing the overlap between the wave functions of the valence-shell electrons.

The band calculations for the metallic phase have shown that the conduction is mainly due to holes in the Ir $5d\varepsilon$ orbital located at the top of the valence band, while the Cu $3d$ orbital is almost completely filled.[8] The NMR of Cu (Ref. 10) and x-ray photoemission spectroscopy[6] (XPS) measurements in the metallic and insulating phases revealed that the valence state of Cu almost approaches to Cu^+, which is consistent with band calculations. Thus it seems probable that the ionic configuration of $Cu^+Ir^{3+}Ir^{4+}S_4^{2-}$ is realized in the insulating state. The ordering of Ir^{3+} and Ir^{4+} ions is a possible origin of the MI transition. Electron diffraction for the LTI phase[11] indicates the superstructure with a unit cell of $2a \times 2a \times 2a$, although the configuration of the ionic order has not been determined. It is to be noticed that an Ir^{4+} ion in the low-spin state has an electronic configuration of $5d_\varepsilon^5 d_\gamma^0$, which is consistent with Jahn-Teller distortion with the stretched c axis.[3] In addition, an Ir^{4+} ion has a moment of $S = 1/2$, while Cu^+ ($3d^{10}$) and Ir^{3+} ($5d_\varepsilon^6 d_\gamma^0$) are nonmagnetic. Therefore, the dimerization of Ir^{4+} ions to form a spin

singlet has been proposed for explaining the nonmagnetic state of the LTI phase. No long-range antiferromagnetic ordering has ever been detected by the NMR measurement.[10] Clear evidence for such ionic order or dimerization, however, has not yet been shown at present.

Some substitutional studies were performed in order to understand the origin of the MI transition. Nagata *et al.*[12] studied Se substitution for S at the *X* site. The result showed that the substitution gradually decreases T_{MI}. Further Se substitution results in a change from a first-order transition to a higher-order one. When the substitution exceeds 80%, the MI transition disappears and the system merely exhibits metallic conduction. The substituted end member $CuIr_2Se_4$ is an analog to $CuRh_2Se_4$, but the former does not show superconductivity above 0.5 K, whereas the latter has been confirmed to be a superconductor with the T_c of 3.48 K.[14] Matsumoto *et al.*[13] carried out a *B*-site substitution, as in $Cu(Ir_{1-x}Rh_x)_2S_4$. It was found that the T_{MI} rapidly decreases with increasing Rh content, suggesting that Ir plays an important role in the MI transition.

We note that the *A*-site substitution should also be significantly important. As shown by the band structure calculation,[8] the electronic state near E_F, which is located near the top of the valence band, is basically composed of Ir $5d$ and S $3p$ electrons. That is to say, the edge-shared IrS_6 octahedron network is mainly responsible for the electrical conduction and the MI transition. The *A*-site substitution takes the advantage of keeping the IrS_6 network hardly changed. This makes it possible to study how the MI transition changes by an excess electron of substituted Zn.

Since Cu/Zn $3d$ and $4s$ bands lie far below and above the E_F, respectively, it is expected that this substitution will introduce electrons at or near the E_F for the metallic cubic system, leading to a hole filling. Moreover, the LTI phase as well as the MI transition will be influenced accordingly, which would reveal some clues to the origin of the MI transition. Our earlier paper[15,16] showed that the substitution strongly suppresses the MI transition and results in the appearance of superconductivity. In this paper, we will present new and comprehensive results on the structural, electrical, and magnetic properties in the $Cu_{1-x}Zn_xIr_2S_4$ system. We will also concern the occurrence of superconductivity as well as the mechanism of the MI transition.

II. EXPERIMENTAL METHODS

Polycrystalline samples of $Cu_{1-x}Zn_xIr_2S_4$ were prepared by chemical reaction in a sealed evacuated quartz ampoule. The starting material was the elements Cu, Zn, Ir, and S with the purity higher than 99.9%. The sealed ampoule was first heated slowly to 1023 K and then fired at 1123–1473 K for 96–120 h, depending on the Zn-doping level. The more Zn is introduced, the higher reaction temperature is necessary. A single phase was successfully obtained for $x \leqslant 0.85$. In the case of $x \geqslant 0.9$, the samples contain impurity phases such as ZnS and Ir_2S_3, though the reaction temperature achieved as high as 1473 K, which is closed to the softening temperature of the quartz glass ampoule. The as-prepared powder was pressed into pellets under pressure of 2000 kg/cm^2, and the pellets were sintered at the same temperature for 48 h. All the samples were furnace cooled after the firing.

Powder XRD was performed at room temperature with Cu $K\alpha$ radiation by employing a RIGAKU x-ray diffractometer. Typically, data were collected with a 2θ step of 0.024°, step time of 2.5 s, and 2θ range of 10°–100°. For the samples of $x=0.1$, 0.2, and 0.3, low-temperature XRD measurements were also carried out at 9 K. The crystal structure was refined by the RIETAN Rietveld analysis program.[17]

The electrical resistivity (ρ) was measured by the standard dc four-probe method down to 0.4 K. The typical dimension of the measured samples is $5\times2\times1$ mm^3. Silver paste was used to make the electrical contacts. In the case of low resistivity for the metallic state, the current was fixed to be 1–5 mA. When the resistivity is relatively high in the insulating state, however, the current was adjusted to keep the measured voltage less than 10 mV. The *I*-*V* relation was checked at some fixed temperatures, which showed up as essentially linear in the measured range. At the low temperatures of 0.4–3 K, where the ^{3}He refrigerator was used, the electrical current was set as 0.01–0.1 mA, avoiding the heating disturbance.

The magnetic susceptibility (χ) was obtained by using a Quantum Design superconducting quantum interference device (SQUID) magnetometer. The measurement was performed for about 100 mg samples during cooling and heating processes between 1.8 K and 300 K under an applied field of 1000 Oe. The measured precision was 10^{-8}–10^{-9} emu. The background was subtracted. In the measurement of the superconducting transition, a low field of 0.1–10 Oe was applied for zero-field-cooling (ZFC) and field-cooling (FC) processes.

III. RESULTS AND DISCUSSION

A. Crystal structures

The crystal structure of the cubic spinel is mainly characterized by the lattice constant *a* and parameter *u*, where *u* gives the exact position for sulfur atoms as (*u*,*u*,*u*). The Rietveld analysis for the room-temperature XRD data demonstrates that the system $Cu_{1-x}Zn_xIr_2S_4$ has the normal spinel structure with Cu/Zn and Ir occupying *A* and *B* sites, respectively. The Cu/Zn occupancies were set to the nominal values. The weighed-pattern factor R_{wp} is about 8%, and the parameter *S*, ''the goodness of fitting,'' is around 1.5, indicating the reliability for the structural refinements. The obtained lattice parameters *a* and *u* are shown in Fig. 1 as a function of Zn content. The lattice constant *a* increases linearly with increasing Zn content until $x=0.85$, in accordance with Vergard's law. Meanwhile the *u* parameter increases a little, suggesting that the IrS_6 octahedron becomes more distorted by the Zn substitution. It is noted that the effective ionic radii for tetrahedrally coordinated Cu^+ and Zn^{2+} are both 0.60 Å.[18] The significant lattice expansion is probably attributed to the hole filling by the Zn substitution, because the holes in the valence band are generally expected to contract the lattice. In fact, the Cu/Zn substitution in other thiospinel systems, such as $(Cu, Zn)Cr_2S_4$, also shows a similar effect.[1]

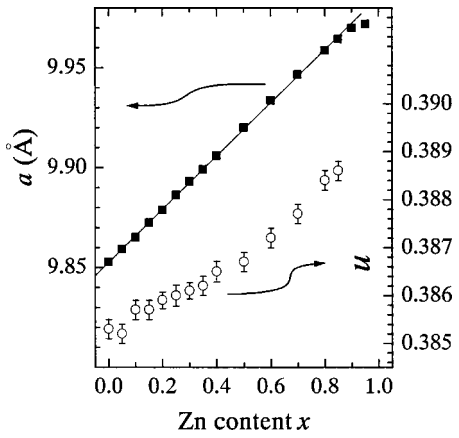

FIG. 1. Variations of the structural parameters a and u of the thiospinel $Cu_{1-x}Zn_xIr_2S_4$ at 295 K upon Zn content x.

The low-temperature XRD for Zn-substituted samples of $x=0.1$, 0.2, and 0.3 indicates a two-phase coexistence below the T_{MI}. Figure 2 shows the XRD pattern in the 2θ range of 35°–50° for $x=0.2$ sample. Apart from the LTI phase, the cubic spinel phase can be identified by the third peak between the split ones around $2\theta=36.11°$ and 47.68°. So a multiphase Rietveld analysis was performed, assuming that the low-temperature cubic (LTC) and LTI phases have the normal cubic and tetragonal[3] spinel structures, respectively. The results are shown in Table I.

Figure 3 shows the axial ratio $c_t/\sqrt{2}a_t(\eta)$ and the molar fraction of the LTI phase (ξ_{LTI}) versus Zn content. The ξ_{LTI} data estimated from the magnetic susceptibility measurements[16] are also presented. As can be seen, at the beginning of the Zn substitution, ξ_{LTI} decreases almost in coincidence with the straight line $1-x$. Then it drops rapidly for $x\geqslant 0.2$. Finally, it becomes zero at $x\sim 0.4$. The axial ratio η decreases gradually with increasing the Zn content. η tends to be 1.0 (no structural deformation) at $x\sim 0.4$ by the extrapolation. In fact, we could not find the existence of the LTI phase for $x>0.4$. The inset shows the MI transition temperature (see the later sections) as a function of η. It can be seen that T_{MI} is closely related to the structural deformation.

It is to be noticed that the LTI phase of $CuIr_2S_4$ probably has the ordering of Ir ions with ionic configuration of

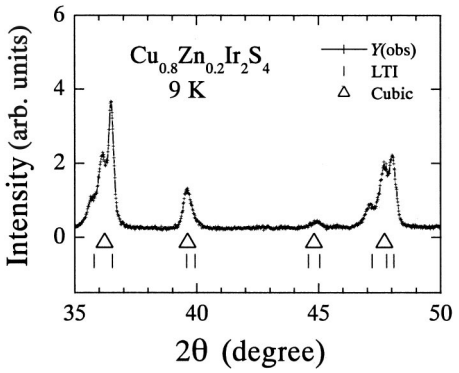

FIG. 2. Part of the XRD pattern for $Cu_{0.8}Zn_{0.2}Ir_2S_4$ at 9 K. The reflection positions for tetragonal and cubic spinel phases are marked by vertical bars and triangles, respectively.

TABLE I. Crystallographic data for the LTI (with space group of $I4_1/amd$) and LTC phases at 9 K, obtained by the multiphase Rietveld analysis. The atomic coordinates for the LTI phase are Cu/Zn($4a$): (0, 0, 0), Ir($8d$): (0, 1/4, 5/8), and S($16h$): (0, y, z). The molar fraction for the LTI phase (ξ_{LTI}) is also presented. In the refinements, B factors for all the ions were fixed to be 0.2 Å^2. The data of the $x=0$ sample were taken for the comparison from Ref. 3.

x	Unit cell Å or Å^3	Atomic coordinates	ξ_{LTI} (%)	R_{wp} (%)	S
0	$a_t=6.8645(4)$				
	$c_t=10.0257(6)$	$y=0.238(4)$			
	$c_t(\sqrt{2}a_t)=1.033$	$z=0.391(2)$	100	11.00	2.52
	$2V_t=944.8(1)$				
0.1	$a_t=6.8975(7)$				
	$c_t=10.017(1)$	$y=0.236(1)$	87.1		
	$c_t/(\sqrt{2}a_t)=1.027$	$z=0.393(1)$			
	$2V_{LTI}=953.1(2)$			12.4	3.42
	$a_c=9.866(1)$				
	$V_{LTC}=960.3(3)$	$u=0.375(3)$			
0.2	$a_t=6.9195(7)$				
	$c_t=9.983(1)$	$y=0.238(1)$	65.3		
	$c_t/(\sqrt{2}a_t)=1.020$	$z=0.3952(8)$			
	$2V_{LTI}=956.0(2)$			11.65	2.66
	$a_c=9.8673(9)$				
	$V_{LTC}=960.7(2)$	$u=0.385(1)$			
0.3	$a_t=6.9613(7)$				
	$c_t=9.941(1)$	$y=0.232(6)$	7.2		
	$c_t/(\sqrt{2}a_t)=1.010$	$z=0.401(3)$			
	$2V_{LTI}=963.4(2)$			7.25	2.43
	$a_c=9.8802(2)$				
	$V_{LTC}=964.49(4)$	$u=0.3865(2)$			

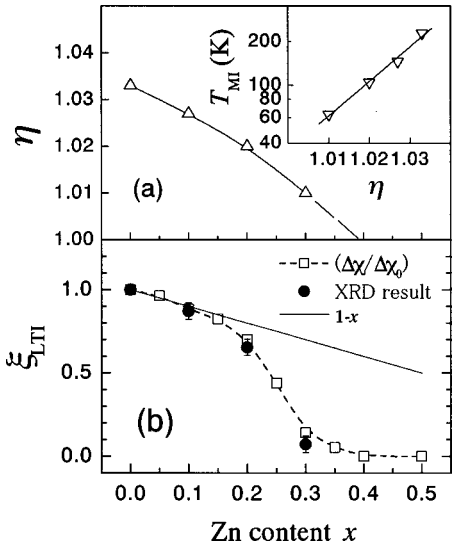

FIG. 3. Axial ratio η (a) and the phase fraction for the LTI phase ξ_{LTI}. (b) vs Zn content in $Cu_{1-x}Zn_xIr_2S_4$ ($0\leqslant x\leqslant 0.5$). The inset shows the MI transition temperature T_{MI} (in a logarithmic scale) as a function of η. The lines are guides to the eye.

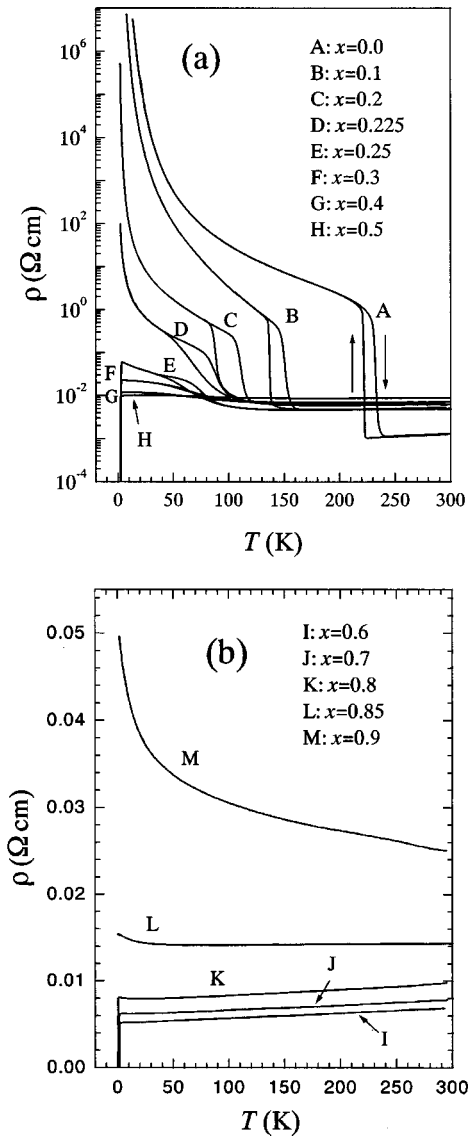

FIG. 4. Temperature dependence of resistivity for $Cu_{1-x}Zn_xIr_2S_4$ [(a) $0 \leqslant x \leqslant 0.5$, (b) $0.6 \leqslant x \leqslant 0.9$] sintered specimen. Note the logarithmic scale for (a).

$Cu^{+}Ir^{3+}Ir^{4+}S_4{}^{2-}$. In case of the LTI phase of $Cu_{1-x}Zn_xIr_2S_4$, similar charge ordering is also expected. In Fig. 3(b), the change of ξ_{LTI}, which is almost equal to $1-x$ in the low-x region, suggests that the Ir^{4+} concentration determines the molar fraction of the LTI phase. Thus it is reasonable to suppose the ionic configuration of the LTI phase as $Cu_{1-x}{}^{+}Zn_x{}^{2+}Ir^{3+}Ir^{4+}S_4{}^{2-}$, which is stabilized by charge segregation accompanied by the phase separation below T_{MI}. That is to say, some electrons in the LTI phase transfer to the LTC phase. This charge disproportion is also supported by the NMR measurement.[19] When further increasing x, however, it becomes difficult to completely maintain the charge disproportion from the viewpoint of charge neutrality. As a balance, the number of transferred electrons and the molar fraction of the LTI phase should be gradually decreased. Finally, the rapid collapse of the LTI phase is expected at a higher Zn concentration. It is worth noting that the LTC phase should be different from the HTM phase due to the charge transference. Further experiments are necessary to confirm this point.

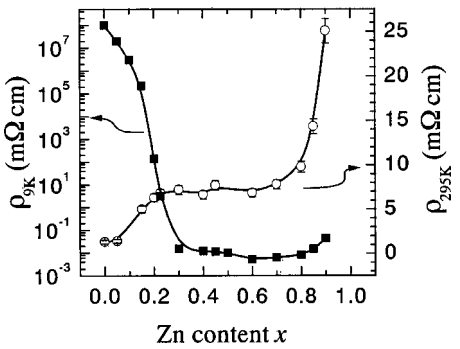

FIG. 5. Resistivity at 9 K (left, in a logarithmic scale) and 295 K (right) as a function of Zn content in $Cu_{1-x}Zn_xIr_2S_4$. The lines are guides to the eye.

B. Electrical resistivity

With regard to the parent compound $CuIr_2S_4$, first of all, the resistivity measurement shows a similar result with previous reports.[2–4] The MI transition is identified by the three orders of magnitude jump in resistivity at about 230 K, as shown by line A of Fig. 4(a). The thermal hysteresis indicates that the phase transition is of first order. The T_{MI} value, defined as the average of the transition midpoints for cooling and heating processes, is determined as 228 K.

The MI transition is suppressed by the Zn substitution, as shown in Fig. 4(a). With the Zn substitution, the MI transition moves towards lower temperatures. The resistivity change at the MI transition becomes smaller and smaller. Apparently, the MI transition disappears for $x \geqslant 0.25$. However, small thermal hysteresis can be observed for $x=0.25$ and 0.3 samples, indicating that the phase transition still takes place. For $x \geqslant 0.4$, the thermal hysteresis cannot be found any more. The sudden resistivity drop around 3 K for $x \geqslant 0.25$ is due to a superconducting transition, which will be discussed in Sec. III E.

We note that the normal-state resistivity shows interesting behavior. For $x=0.3$ sample, the negative temperature coefficient of resistivity (TCR) occurs at about 200 K, which is significantly higher than the T_{MI} (around 70 K). In the case of $x=0.4$ and 0.5, where the MI transition is completely suppressed, the $\rho(T)$ curve also shows a hump at low temperatures. For the $x=0.6$ and 0.7 samples, however, the TCR keeps positive. The $\rho(T)$ curve is essentially linear for $T > 50$ K, but follows the power law $\rho(T)=\rho_0+\beta T^n$, in the range of $4.5\,\mathrm{K} < T < 50\,\mathrm{K}$. The fitted result shows $n=1.5$ and 2.3 for $x=0.6$ and 0.7, respectively. Further increasing Zn content results in the disappearance of superconductivity, and the negative TCR appears again.

Considered the hole filling by the Zn substitution, the hole concentration n_h for $Cu_{1-x}Zn_xIr_2S_4$ is expected to be $1-x$ per unit formula. Thus an insulating state is expected for $x=1$, since the $5d\varepsilon$ orbital of Ir is fully occupied. As can be seen in Fig. 5, the room-temperature resistivity ($\rho_{295\,\mathrm{K}}$) in-

creases with increasing x, consistent with the hole-filling picture. The metal-to-insulator crossover at $x \sim 0.85$, shown in Fig. 4(b), is probably due to the Anderson localization effect.

Figure 5 also shows the low-temperature resistivity at 9 K as a function of x. An abrupt decrease in resistivity at $x \sim 0.25$ can be seen, indicating an insulator-to-metal transition. We attribute this transition to a percolation effect. As revealed by the XRD result, the LTC phase coexists with the LTI phase at low temperature for $x=0.1$, 0.2, and 0.3 samples. The samples of $x=0.1$ and 0.2 mainly contain the LTI phase, and the dominant phase for $x=0.3$ is the LTC phase. Remember that the high-temperature cubic (HTC) phase shows metallic conduction for $x<0.85$. It is reasonable that the LTC phase around $x \sim 0.25$ is metallic. Therefore, the insulator-to-metal transition at $x \sim 0.25$ is virtually a kind of percolation transition. The percolation threshold seems to be $\xi_{\mathrm{LTI}} \sim 0.5$ at $x \sim 0.25$, according to Fig. 3(b), in this system.

Analysis of the low-temperature conductivity may give useful information on the LTI phase. Hagino *et al.*[4] analyzed the low-temperature resistivity for $CuIr_2S_4$ in terms of the thermal activation mechanism. The activation energy (E_a) was calculated as 0.047 eV using the data in temperature range of 140–200 K. Actually, the conductivity (σ) does not essentially obey the Arrhenius expression $A \exp(-E_a/kT)$ in a wide temperature range. Burkov *et al.*[20] reported that the resistivity below 50 K could be best fitted by a hopping conductivity $\sigma=\sigma_0 \exp[-(T_0/T)^{\alpha}]$, with $\alpha=1/2$. This implies that the E_F locates at a localized state, which is inconsistent with the band-gap opening result.[6]

We tried to analyze the low-temperature conductivity in a different way. As for the electronic state of the LTI phase, we suppose the existence of localized states with different energy levels around E_F due to the lattice imperfections. So conductivity for the LTI phase basically comes from the thermal excitation of carriers from the top of the valence band and the variable-range hopping (VRH) of the localized carriers. The first contribution can be expressed as $\sigma_1=A \times \exp(-E_a/kT)$. The second one is considered as a three-dimensional VRH conductivity $\sigma_2=B \exp[-(T_0/T)^{1/4}]$.[21] Neglecting the influence of the LTC phase, therefore, we may make a data fitting by the equation

$$\sigma=\sigma_1+\sigma_2=A \exp(-E_a/kT)+B \exp[-(T_0/T)^{1/4}]. \quad (1)$$

It is found that the low-temperature $\sigma(T)$ data can be well fitted. So the single-hopping conductivity $\sigma_0 \exp[-(T_0/T)^{1/2}]$ is not necessarily essential. Figure 6 shows the data fitting for the parent compound. It is clear to see that σ_1 and σ_2 are both necessary to present a good fitting. Table II lists the fitted results. The E_a value for $CuIr_2S_4$ is 0.019 eV. This result seems to be quite consistent with the photoemission spectrum study, which shows a $\sim$20 meV gap between E_F and the top of the valence band.[6] In Fig. 7, it is shown that E_a decreases with increasing Zn content. E_a tends to be zero at $x \sim 0.25$. In the inset, one can see that E_a rapidly decreases with decreasing the structural distortion.

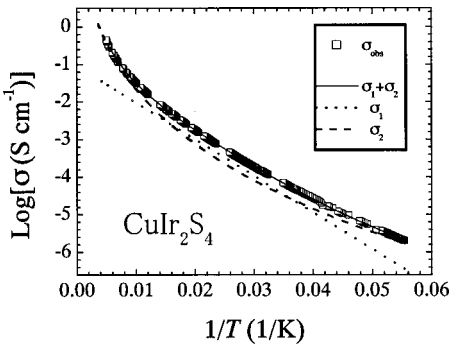

FIG. 6. The data fitting for $\sigma(T)$ of $CuIr_2S_4$ using Eq. (1), indicating that both σ_1 and σ_2 are necessary to make a good fitting. Some data points of σ_{obs} are absent in order to show the line $\sigma_1+\sigma_2$.

C. Magnetic susceptibility

Figure 8 shows the temperature dependence of magnetic susceptibility for $Cu_{1-x}Zn_xIr_2S_4$ samples. With decreasing temperature, the parent compound undergoes a transition from paramagnetism to diamagnetism at 224 K. A thermal hysteresis is obvious at the transition, and the T_{MI} value (the average of the transition midpoint temperatures for cooling and heating) was also 228 K. The weak paramagnetism above T_{MI} is interpreted as the Pauli paramagnetism of conduction electrons. Therefore, the susceptibility drop ($\Delta\chi$) at T_{MI} is believed to be due to the quenching of the Pauli paramagnetism by a gap opening at E_F. The weak positive temperature dependence of susceptibility indicates a positive $d^2N(E)/dE^2$ at E_F. The diamagnetism with the minimum susceptibility χ_{min} of -6.29×10^{-5} emu/mol in the insulating state mainly originates from the ion core contribution.[22] With further decreasing temperature, χ has a small upturn, which was attributed to the lattice imperfections with magnetic moment.[2–4] The corresponding magnetic moment is determined to be $0.024\mu_B$ per formula by a Curie-Weiss fitting.

With increasing Zn content, the $\chi(T)$ changes systematically. First, T_{MI} decreases rapidly, consistent with result of

TABLE II. Fitted results for the $\rho(T)$ data of $Cu_{1-x}Zn_xIr_2S_4$ using Eq. (1).

x	0	0.05	0.1	0.15	0.2	0.225
Fitting range (K)	18–190	20–150	8–80	4.2–80	2–80	2–45
A (S cm^{-1})	0.091	0.0104	0.00233	0.0278	0.104	0.151
E_a (eV)	0.0193	0.0192	0.0084	0.0054	0.0023	0.0009
B (S cm^{-1})	1.05×10^6	5.2×10^9	2.6×10^6	5.7×10^5	1.3×10^4	620
T_0 (K)	9.8×10^6	4.58×10^7	7.1×10^6	2.96×10^6	5.1×10^5	3.3×10^4

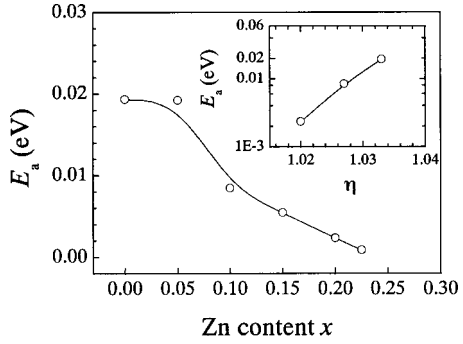

FIG. 7. The extracted activation energy E_a vs Zn content in $Cu_{1-x}Zn_xIr_2S_4$ ($0 \leqslant x \leqslant 0.225$). The inset shows the dependence of axial ratio η in a logarithm scale. The lines are guides to the eye.

the resistivity measurement. At the same time, $\Delta\chi$ becomes smaller and smaller. The signal of the phase transition does not disappear until $x \geqslant 0.4$. The upturn of χ at low temperature is also attributed to the extrinsic magnetic moment, because the magnetic moment is rather small [$(0.02-0.08)\mu_B$; see Table III] and seems to have no systematic change upon Zn substitution. The abrupt drop of χ at about 3 K for $x > 0.2$ samples is due to a superconducting transition.

Second, the room-temperature susceptibility $\chi_{300\,\mathrm{K}}$ decreases monotonically with increasing Zn substitution, as clearly shown in Fig. 9. This result indicates that the Pauli paramagnetic susceptibility χ_{Pauli} decreases with increasing x. Since χ_{Pauli} can be expressed by $\mu_B^2 N(E_F)$, the decrease of χ_{Pauli} reflects the decrease of $N(E_F)$. Since E_F is located at the top of the valence band, we may conclude that the Zn substitution raises the chemical potential, as expected in the Introduction. In other words, the Zn substitution truly induces a hole filling for the metallic state.

Third, χ_{min} goes up with increasing x for $x < 0.4$. As stated in the above sections, these samples contain LTI and LTC phases below T_{MI}. Here we supposed that the LTC phase is basically a metal, which contributes Pauli paramagnetism. So the increase of χ_{min} corresponds to the increase of ξ_{LTC} ($\xi_{\mathrm{LTC}} = 1 - \xi_{\mathrm{LTI}}$). Or the decrease of $\Delta\chi$ represents the decrease of ξ_{LTI}. Based on this point, we previously developed a method to estimate the phase fraction.[16] ξ_{LTI} was *roughly* calculated as the ratio of the observed susceptibility drop $\Delta\chi$ to the assumed one $\Delta\chi_0$ for a complete phase transition. $\Delta\chi_0$ was the extrapolated susceptibility of the metallic state at T_{MI} subtracted by χ_{min} of $CuIr_2S_4$, as shown in Fig. 8. The result was in good agreement with that of the XRD Rietveld analysis (see Fig. 3).

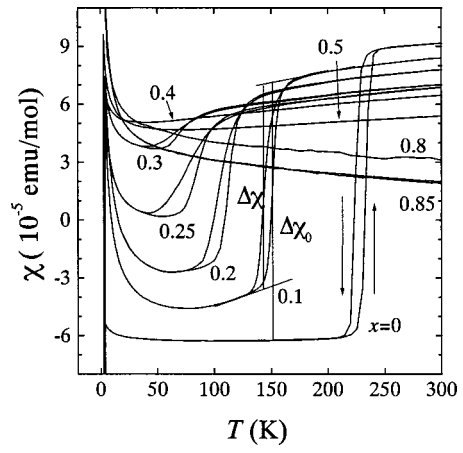

FIG. 8. Temperature dependence of magnetic susceptibility for $Cu_{1-x}Zn_xIr_2S_4$ powdered samples. The applied field is 1000 Oe. Here $\Delta\chi$ and $\Delta\chi_0$ are marked.

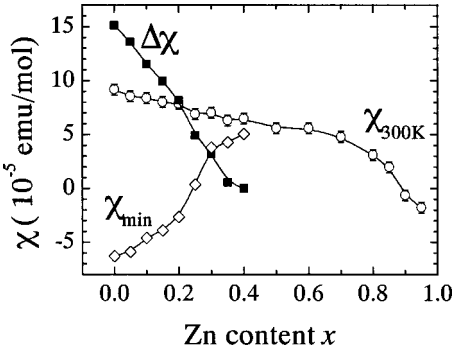

FIG. 9. Room-temperature susceptibility ($\chi_{300\,\mathrm{K}}$), the change of susceptibility at T_{MI}($\Delta\chi$), and the minimum susceptibility (χ_{min}) vs Zn content x in $Cu_{1-x}Zn_xIr_2S_4$. The lines are guides to the eye.

We notice that the low-temperature $\chi(T)$ shows a weak temperature dependence after subtracting the Curie-Weiss contribution χ_{CW}. Below T_{MI}, the subtracted χ is found to increase with increasing temperature. This is more obvious for the Zn-substituted samples. As for the LTI phase, the electronic configurations of Ir^{4+} are expected to be magnetic ($d_\varepsilon^5 d_\gamma^0$, $S=1/2$), while Ir^{3+} is nonmagnetic ($d_\varepsilon^6 d_\gamma^0$, $S=0$). Thus, for explaining the nonmagnetic state, it is reasonable to assume that Ir^{4+} ions form spin-singlet pairs, similarly to the case in Ti_4O_7.[23] If so, the thermal breaking of the Ir^{4+} pairs may account for the temperature dependence of the subtracted χ.

The low-temperature $\chi(T)$ can be quantitatively analyzed as follows. The total susceptibility χ_{tot} includes χ_{core}, χ_{Pauli}, and χ_{Landau}, Van Vleck susceptibility χ_{VV}, χ_{CW}, and the thermally excited susceptibility χ_{excited}. The first four terms are approximately temperature independent. χ_{excited} can be expressed as $n\mu_0\mu_J^2/(3k_BT)$, where n refers to the number of excited Ir^{4+} and μ_J is the effective magnetic moment. Since only the LTI phase contributes the χ_{excited}, n is given as $N_A\xi_{\mathrm{LTI}}\exp(-\Delta/k_BT)$, where N_A is the Avogadro constant and Δ is the energy to activate *one* localized spin. The exchange energy J in a Ir^{4+} dimer will be twice of Δ. Therefore,

$$\chi_{\mathrm{tot}} = \chi_0 + C_1/(T-\theta) + (C_2/T)\exp(-\delta/k_BT), \qquad (2)$$

where $\chi_0 = \chi_{\mathrm{core}} + \chi_{\mathrm{Pauli}} + \chi_{\mathrm{Landau}} + \chi_{\mathrm{VV}}$. The magnetic moment due to the lattice imperfections μ_{im} and the effective magnetic moment μ_J of excited Ir^{4+} can be calculated from the fitted C_1 and C_2 values, respectively.

The data-fitting results are listed in Table III. Basically, χ_0 increases with increasing x, mainly due to the increase of the fraction of LTC phase. μ_J is around $0.6\mu_B$, which is obviously smaller than the ideal value $1.73\mu_B$ for Ir^{4+}. This implies that the excited Ir^{4+} with spin 1/2 is not so stable, and

TABLE III. Fitted results for the $\chi(T)$ data of $Cu_{1-x}Zn_xIr_2S_4$ using Eq. (2).

x	0	0.05	0.1	0.15	0.2	0.25
Fitting range (K)	4.5–200	4.5–145	4.5–115	4.5–100	4.5–70	4.5–40
$\chi_0(10^{-5}$ emu/mol)	−6.348	−6.38	−6.215	−5.795	−3.962	−1.54
$\mu_{\rm im}(\mu_B)$	0.024	0.054	0.068	0.078	0.074	0.052
θ (K)	−3.6	−0.08	−1.0	−1.2	−1.7	−1.3
$\mu_J(\mu_B)$	0.56	0.58	0.67	0.63	0.69	1.03
Δ (eV)	0.084	0.047	0.039	0.034	0.031	0.026

some of the Ir^{4+} may be kinetically delocalized through the process $Ir^{4+}+Ir^{3+}\rightarrow Ir^{3+}+Ir^{4+}$. It is noted that J decreases monotonically with increasing Zn content, as shown in Fig. 10. Since the Zn substitution decreases the axial ratio, the decrease of J should be related to the decrease of the lattice distortion. One may expect that the lattice deformation shortens the Ir^{4+}-Ir^{4+} distance and thus enhances J. The inset of Fig. 10 shows the J dependence of $T_{\rm MI}$. Their close relation suggests that the Ir^{4+} dimerization be important to the MI transition.

D. Origin of the MI transition

In view of the ionic model for the LTI phase of $CuIr_2S_4$, it seems most probable that the ionic configuration of $Cu^{+}Ir^{3+}Ir^{4+}S_4^{2-}$ is realized in the insulating state. The ordering of charges on the Ir site is one possible origin of the MI transition. In addition, the absence of intrinsic local magnetic moments for the LTI phase suggests the dimerization of Ir^{4+} with spin singlet.

In the HTM phase, the valence electrons hop from one site to another in an electron transport process. If the kinetic energy (t) for the electrons is larger than the energy cost for the hopping, the material will have metallic conduction. Otherwise, it will exhibit insulating property. In the $Cu_{1-x}Zn_xIr_2S_4$ system, the main hopping route is within the IrS_6 network. One possible hopping process is $Ir^{4+}+Ir^{3+}\rightarrow Ir^{3+}+Ir^{4+}$, which costs the energy of the interatomic Coulomb repulsion (U_i) for the cubic phase. The other possibility $Ir^{4+}+Ir^{4+}\rightarrow Ir^{3+}+Ir^{5+}$ takes the on-site Coulomb correlation energy (U_0) besides U_i. Since U_0 is generally much greater than U_i, just the former process should be taken into considerations. The metallic conduction of the cubic spinel phase can be understood by supposing $t > U_i$.

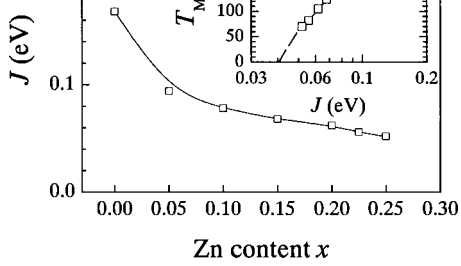

FIG. 10. Relation between the MI transition temperature $T_{\rm MI}$ and the exchange energy for assumed Ir^{4+} dimers J (in a logarithmic scale) in $Cu_{1-x}Zn_xIr_2S_4$ ($0\leqslant x\leqslant 0.25$). The lines are guides to the eye.

With regard to the LTI phase, however, the carrier hopping definitely breaks the Ir^{4+} dimers, irrespective of the structural details. So the hole hopping from Ir^{4+} to the neighbor Ir^{3+} through the intermediate S atoms needs the energy $U_{\rm eff}=U_i+J$. In this circumstance, $t<U_{\rm eff}$ is plausible, resulting in the insulating ground state for the LTI phase. It is pointed out that, according to this model, the driving force for the MI transition comes from the interatomic Coulomb interaction *and* the dimerization of Ir^{4+}.

The present results show the following effects of substituting Cu by Zn on the MI transition. (a) The Zn substitution fills the hole carriers for the HTM phase. The metallic conduction originates from the hybridization states between Ir $5d\varepsilon$ and S $3p$. (b) The MI transition is closely related to the structural deformation. It is found that $T_{\rm MI}$, E_a, and J all increase with increasing the structural distortion. (c) The phase separation below $T_{\rm MI}$ indicates that the LTI phase favors an equal number of Ir^{3+} and Ir^{4+}, which supports the idea of charge ordering at the B site. The extracted exchange energy J is strongly correlated with $T_{\rm MI}$, revealing the important role of dimerization. Thus the results are understood by the model of Ir^{4+} dimerization.

A spin-singlet dimerization has been found in well-characterized Ti_4O_7.[23] In that Ti^{3+} dimer, weak direct chemical bonding was proposed as the σ overlap between the two d orbitals. The Ti^{3+} pairs were considered as bipolarons. In the $CuIr_2S_4$-related system, similar cases are also expected.

The unusual pressure effect[3,9] can be tentatively interpreted in terms of the above model. Under external pressure, though t is increased by increasing the related orbital overlap, the exchange interaction J may be increased more due to the shortening of the Ir^{4+}-Ir^{4+} bond length, which makes the carrier hopping more difficult. So the applied pressure may stabilize the insulating state. The chemical pressure effect, shown in the $CuIr_2(S_{1-x}Se_x)_4$ system,[12] may also be explained. The Se substitution increases the nearest Ir-Ir distance, which leads to the rapid decrease of J. Therefore, the MI transition related to the structural deformation is seriously depressed by the Se substitution.

E. Superconductivity in $Cu_{1-x}Zn_xIr_2S_4$ ($0.25\leqslant x\leqslant 0.8$)

The thiospinels are seldom superconductive. To our knowledge, $CuRh_2S_4$ is a unique superconductor that has

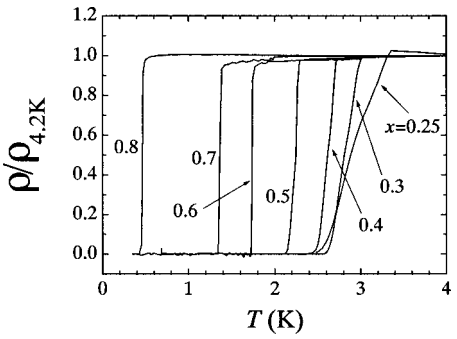

FIG. 11. Temperature dependence of the reduced resistivity $\rho/\rho_{4.2\,\mathrm{K}}$ in $Cu_{1-x}Zn_xIr_2S_4$ ($0.25 \leqslant x \leqslant 0.8$), showing the superconducting transition.

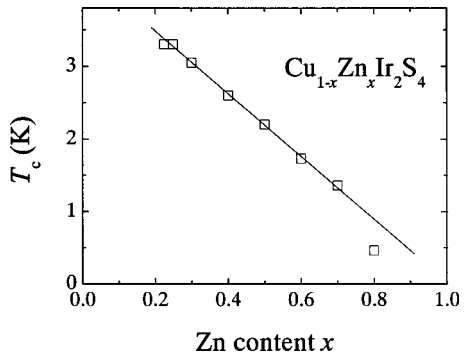

FIG. 13. Superconducting transition temperature as a function of Zn content in $Cu_{1-x}Zn_xIr_2S_4$.

ever been confirmed.[14] Since Ir is just below Rh in the periodic table, one may expect that $CuIr_2S_4$ should have similar electronic states and physical properties as those of $CuRh_2S_4$. However, the ground state of $CuIr_2S_4$ is an insulator due to the MI transition at 228 K. By suppression of the MI transition through Zn substitution, we previously found the superconductivity in the $Cu_{1-x}Zn_xIr_2S_4$ system.[15,24]

Figure 11 shows the superconducting transition in the resistivity measurement for $Cu_{1-x}Zn_xIr_2S_4$. The reduced ρ was adopted for the convenience of comparison. For $x=0.25$ and 0.3 samples, in which the insulating phase was incorporated, the transition is rather broad. They seem to have two transitions, which are due to the percolation effect. The other samples with higher Zn content have a relatively sharp transition. The Meissner effect has been observed by dc magnetization measurements under 10 Oe with field cooling.[24] The previous result showed a very low Meissner volume fraction (~1% at 1.8 K). When the applied field is decreased, the Meissner effect can be significantly enhanced. Figure 12 shows the temperature dependence of the dc susceptibility under different magnetic fields for the $Cu_{0.6}Zn_{0.4}Ir_2S_4$ powdered sample. The Meissner volume fraction achieves 16.5% under 0.1 Oe at 1.8 K demonstrating the bulk superconductivity.

Figure 13 shows the superconducting transition temperature T_c as a function of Zn content in $Cu_{1-x}Zn_xIr_2S_4$. Here T_c was determined as the onset transition temperature in the magnetic susceptibility (for $T_c > 1.9$ K) or the transition midpoint temperature in the resistance (for $T_c < 1.9$ K). It can be seen that T_c decreases almost linearly with decreasing Zn content. The extrapolated T_c value for $CuIr_2S_4$ is 4.3 K closed to the T_c of $CuRh_2S_4$ (4.7 K). According to the well-known BCS theory, $T_c \propto \theta_D \exp[-1/VN(E_F)]$, where θ_D is the Debye temperature and V is the electron-phonon interaction. Since $N(E_F)$ decreases with increasing Zn concentration, T_c accordingly decreases if roughly assuming that θ_D and V do not change so much against x.

Figure 14 shows the magnetization as a function of magnetic field at 2.0 K for a $Cu_{0.7}Zn_{0.3}Ir_2S_4$ powdered sample. It can be seen that the compound is a type-II superconductor with $H_{c1}=300$ Oe and $H_{c2}=2.0$ T at 2.0 K. Here $H_{c2}(0)$ can be estimated as ~3.5 T from the equation $H_{c2}(0) = 0.693 T_c(-dH_{c2}/dT)_{T=T_c}$, if assuming the dirty limit.

The occurrence of superconductivity in the $Cu_{1-x}Zn_xIr_2S_4$ system deserves further discussion. As a striking contrast, metallic phase $CuIr_2Se_4$ lacks superconductivity above 0.5 K,[12] and the Ir doping seriously depresses the superconductivity in $Cu(Rh_{1-x}Ir_x)_2S_4$.[13] In addition, the normal-state resistivity for $x=0.3-0.5$ samples of $Cu_{1-x}Zn_xIr_2S_4$ exhibits negative TCR, which suggests the modification of electronic states. From an extrapolation in Fig. 10, one may expect that $J \sim 0.04$ eV for $x=0.3-0.5$. So one possible mechanism is that the Ir^{4+} dimers or spin-singlet bipolarons are more or less formed, resulting in the negative TCR. The bipolaron concentration should be rather small; otherwise, a substantial magnetic susceptibility drop would have been observed when the negative TCR appears.

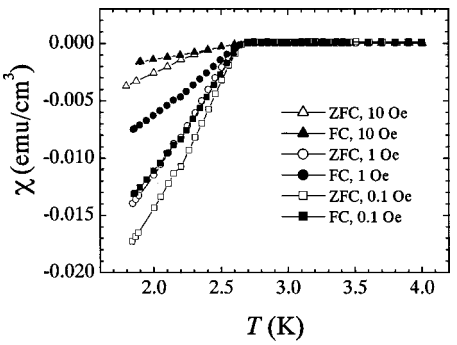

FIG. 12. dc Meissner effect under different magnetic fields for the powdered $Cu_{0.6}Zn_{0.4}Ir_2S_4$ sample.

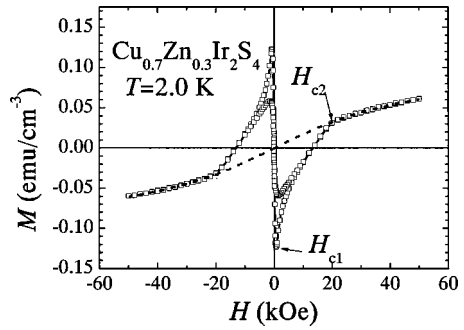

FIG. 14. Magnetization as a function of applied magnetic field for the $Cu_{0.7}Zn_{0.3}Ir_2S_4$ powdered sample. The dashed line refers to the impurity paramagnetism with the Brillouin function.

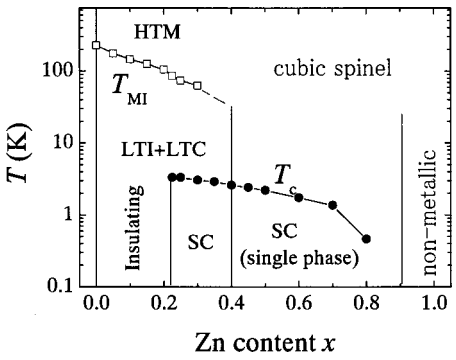

FIG. 15. Phase diagram of $Cu_{1-x}Zn_xIr_2S_4$ ($0 \leqslant x \leqslant 0.9$). The logarithm was used for the temperature axis in order to show the low-temperature phases. Nonmetallic behavior is expected for $0.9 \leqslant x \leqslant 1.0$. The abbreviations are used as follows. HTM: high-temperature metallic. LTI: low-temperature insulating. LTC: low-temperature cubic. SC: superconducting.

Meanwhile, the bipolarons should have a dynamic character due to the thermal fluctuation. In Ti_4O_7, the high-temperature insulating and low-temperature insulating phases are described as the bipolaron liquid and bipolaron crystal, respectively.[25] The bipolaron crystal has long-range-ordered Ti^{3+} dimers, whereas the bipolaron liquid does not. Accordingly, if a few dynamic Ir^{4+} dimers exist in the negative TCR regime, the states can be regarded as a bipolaron gas. Furthermore, it would be of great interest whether the bipolaron gas plays a role in the occurrence of superconductivity. Nevertheless, it should be pointed out that, apart from the formation of the bipolaron gas, other possibilities such as the formation of a charge (spin) density wave cannot be ruled out.

IV. SUMMARY

As a conclusion for the Zn substitution, we drew the phase diagram shown in Fig. 15. Structurally, there are two phases in the system: one is the normal cubic spinel the other is the deformed spinel with lower symmetry. The Zn substitution decreases the hole concentration for the cubic phase. Metallic conduction holds for the cubic spinel except that the carrier concentration is decreased so much that Anderson localization would take place. The T_{MI} is decreased by the Zn substitution. The HTM phase transforms into the LTI and LTC phases at T_{MI} for $x < 0.4$. Below T_{MI}, an insulator-to-metal transition occurs at $x \sim 0.25$ due to the percolation effect. The cubic phase exhibits superconductivity for $0.25 \leqslant x \leqslant 0.8$. The T_c is found to decrease with increasing Zn content.

The origin of the MI transition is tentatively explained. The LTI phase is suggested to be charge ordered with the formation of spin-singlet Ir^{4+} dimers. The interatomic Coulomb repulsion and the exchange interaction in Ir^{4+} dimers are proposed to be responsible for the MI transition. Based on this model, the unusual pressure effect can be basically understood.

The normal-state $\rho(T)$ for $x = 0.3-0.5$ samples shows negative TCR, which suggests modification of the electronic states. One possible explanation is that the negative TCR state involves the formation of bipolaron gas, which might be related to the occurrence of superconductivity. Further investigations are needed to clarify this important issue.

ACKNOWLEDGMENTS

The authors would like to thank Dr. T. Sato for help with the magnetic measurements. Thanks are also due to Professor S. Nagata for helpful discussions.

*On leave from the Department of Physics, Zhejiang University, Hangzhou 310027, China.

†Author to whom correspondence should be addressed. FAX: +81-298-592801. Electronic address: kitazawa.Hideaki@nims.go.jp

[1] R. P. Van Stapele, in *Ferromagnetic Materials*, edited by E. P. Wohlfarth (North-Holland, Amsterdam, 1982), Vol. 3, pp. 603–745.

[2] S. Nagata, T. Hagino, Y. Seki, and T. Bitoh, Physica B **194–196**, 1077 (1994).

[3] T. Furubayashi, T. Matsumoto, T. Hagino, and S. Nagata, J. Phys. Soc. Jpn. **63**, 3333 (1994).

[4] T. Hagino, T. Toji, T. Atake, and S. Nagata, Philos. Mag. B **71**, 881 (1995).

[5] H. Ishibashi, T. Sakai, and K. Nakahigashi, J. Magn. Magn. Mater. **226–230**, 233 (2001).

[6] J. Matsuno, T. Mizokawa, A. Fujimori, D. A. Zatsepin, V. R. Galakhov, E. Z. Kurmaev, Y. Kato, and S. Nagata, Phys. Rev. B **55**, R15 979 (1997).

[7] M. Hayashi, M. Nakayama, T. Nanba, T. Matsumoto, J. Tang, and S. Nagata, Physica B **281&282**, 631 (2000).

[8] T. Oda, M. Shirai, N. Suzuki, and K. Motizuki, J. Phys.: Condens. Matter **7**, 4433 (1995).

[9] G. Oomi, T. Kagayama, I. Yoshida, T. Hagina, and S. Nagata, J. Magn. Magn. Mater. **140–144**, 157 (1995).

[10] K. Kumagai, S. Tsuji, T. Hagino, and S. Nagata, in *Spectroscopy of Mott Insulators and Correlated Metals*, edited by A. Fujimori and Y. Tokura (Springer-Verlag, Berlin, 1995), p. 255.

[11] W. Sun, T. Kimoto, T. Furubayashi, T. Matsumoto, S. Ikeda, and S. Nagata, J. Phys. Soc. Jpn. **70**, 2817 (2001).

[12] S. Nagata, N. Matsumoto, Y. Kato, T. Furubayashi, T. Matsumoto, J. P. Sanchez, and P. Vulliet, Phys. Rev. B **58**, 6844 (1998).

[13] N. Matsumoto, R. Endoh, S. Nagata, T. Furubayashi, and T. Matsumoto, Phys. Rev. B **60**, 5258 (1999).

[14] For a newer reference, see T. Hagino, Y. Seki, N. Wada, S. Tsuji, T. Shirane, K. Kumagai, and S. Nagata, Phys. Rev. B **51**, 12 673 (1995).

[15] H. Suzuki, T. Furubayashi, G. Cao, H. Kitazawa, A. Kamimura, K. Hirata, and T. Matsumoto, J. Phys. Soc. Jpn. **68**, 2495 (1999).

[16] G. Cao, H. Suzuki, T. Furubayashi, H. Kitazawa, and T. Matsumoto, Physica B **281&282**, 636 (2000).

[17] F. Izumi, in *The Rietveld Method*, edited by R. A. Young (Oxford University Press, Oxford, 1993), Chap. 13; Y.-I. Kim and F. Izumi, J. Ceram. Soc. Jpn. **102**, 401 (1994).

[18] R. D. Shannon, Acta Crystallogr., Sect. A **32**, 751 (1976).

[19] A. Goto, T. Shimizu, G. Cao, H. Suzuki, H. Kitazawa, and T. Matsumoto, J. Phys. Soc. Jpn. **70**, 9 (2001). The Cu NMR of the LTI phase of $Cu_{1-x}Zn_xIr_2S_4$ ($0 \leqslant x \leqslant 0.3$) samples shows almost the same Knight shift, indicating that the electronic state in the LTI phase hardly changes by the Zn substitution. So the Zn substitution for Cu does not induce electron carriers for the LTI phase as usual. The induced electrons are expected to transfer into the LTC phase.

[20] A. T. Burkov, T. Nakama, K. Shintani, K. Yagasaki, N. Matsumoto, and S. Nagata, Physica B **281&282**, 629 (2000).

[21] N. F. Mott, J. Non-Cryst. Solids **1**, 1 (1968).

[22] E. König and G. König, in *Landolt-Börnstein Numerical Data and Functional Relationships in Science and Technology*, edited by K.-H. Hellwege, Landolt-Börnstein, New Series, Group II, Vol. 8 (Springer-Verlag, Berlin, 1976), p. 27.

[23] S. Lakkis, C. Schlenker, B. K. Chakraverty, R. Buder, and M. Marezio, Phys. Rev. B **14**, 1429 (1976).

[24] G. Cao, H. Kitazawa, H. Suzuki, T. Furubayashi, K. Hirata, and T. Matsumoto, Physica C **341–348**, 735 (2000).

[25] K. Kobayashi, T. Susaki, A. Fujimori, T. Tonogai, and H. Takagi, cond-mat/9909189 (unpublished).